Excitation of Highly Conjugated (Porphinato)palladium(II) and (Porphinato)platinum(II) Oligomers Produces Long-Lived, Triplet States at Unit Quantum Yield That Absorb Strongly over Broad Spectral Domains of the NIR[†]

Timothy V. Duncan,[‡,§] Paul R. Frail,[‡] Ivan R. Miloradovic,[‡] and Michael J. Therien*,[‖]

Department of Chemistry, University of Pennsylvania, Philadelphia, Pennsylvania 19104-6323, and Department of Chemistry, French Family Science Center, Duke University, Durham, North Carolina 27708-0354

Transient dynamical studies of bis[(5,5′-10,20-bis(2,6-bis(3,3-dimethylbutoxy)phenyl)porphinato)palladium(II)] ethyne (**PPd₂**), 5,15-bis{[(5′-10,20-bis(2,6-bis(3,3-dimethylbutoxy)phenyl)porphinato)palladium(II)]ethynyl}(10,20-bis(2,6-bis(3,3-dimethylbutoxy)phenyl)porphinato)palladium(II) (**PPd₃**), bis[(5,5′-10,20-bis(2,6-bis(3,3-dimethylbutoxy)phenyl)porphinato)platinum(II)]ethyne (**PPt₂**), and 5,15-bis{[(5′-10,20-bis(2,6-bis(3,3-dimethylbutoxy)phenyl)porphinato)platinum(II)]ethynyl}(10,20-bis(2,6-bis(3,3-dimethylbutoxy)phenyl)porphinato)platinum(II) (**PPt₃**) show that the electronically excited triplet states of these highly conjugated supermolecular chromophores can be produced at unit quantum yield via fast $S_1 \rightarrow T_1$ intersystem crossing dynamics (τ_{isc}: 5.2–49.4 ps). These species manifest high oscillator strength $T_1 \rightarrow T_n$ transitions over broad NIR spectral windows. The facts that (i) the electronically excited triplet lifetimes of these **PPd$_n$** and **PPt$_n$** chromophores are long, ranging from 5 to 50 μs, and (ii) the ground and electronically excited absorptive manifolds of these multipigment ensembles can be extensively modulated over broad spectral domains indicate that these structures define a new precedent for conjugated materials featuring low-lying $\pi-\pi^*$ electronically excited states for NIR optical limiting and related long-wavelength nonlinear optical (NLO) applications.

1. Introduction

Organic materials that can attenuate the intensity of sudden strong pulses of light are an important means to protect sensitive optical devices. There is keen interest in the development of optical power limiting (OPL) materials that function over the 750–1600 nm spectral regime of the near-infrared (NIR), as this wavelength domain encompasses the primary emission lines of a variety of important lasing media (Ti:sapphire, Nd:YAG, Nd:YLF, GaAs, GaAlAs, InGaAs, krypton, HeNe, argon, Cr: Forsterite, and Er:glass), as well as the important telecommunication wavelengths. While there are many physical mechanisms that can give rise to OPL, one of the most important is reverse saturable absorption (RSA).[1,2] Materials exhibiting RSA possess strong excited-state absorptive cross sections and weak ground-state absorptive intensity over the spectral window of interest for optical limiting. The additional requirements of a long excited-state lifetime, high resistance to degradative photochemistry, and large magnitude nonlinear optical (NLO) response have made identification of OPL candidates based on RSA for the NIR difficult. In contrast, a wide variety of optical limiting materials based upon phthalocyanine,[3–11] porphyrin,[12–14] fullerene,[15–20] carbon nanotube,[9,21–25] nanoparticle,[26–34] and other[35–40] motifs have been identified for the visible spectral region. The limited number of potential NIR OPL materials[39,41–48] elucidated to date derives largely from the fact that most compounds that possess excited states that absorb strongly in the NIR also manifest diminished excited-state lifetimes due to increased rates of nonradiative relaxation from their respective low-lying excited electronic states.[49–51]

The simultaneous requirements of a long ($> \mu$s) excited-state lifetime, substantial photostability, and broad, high oscillator strength excited-state absorptivity in the NIR, have led to the development of supermolecular chromophores that manifest coupled-oscillator photophysics and extensively delocalized low energy excited triplet (T_1) states characterized by substantial charge-separated (CS) character.[52,53] While these highly conjugated charge-transfer chromophores define new benchmarks for NIR optical limiting,[52,53] it remains an open question whether conjugated materials that feature low-lying electronically excited states that are predominantly $\pi-\pi^*$ in nature can manifest similar T_1-state lifetimes and NIR absorptive characteristics. We report herein highly conjugated palladium(II)- (**PPd$_n$**) and platinum(II)-containing (**PPt$_n$**) porphyrin arrays (Chart 1) that exhibit near-unity $S_1 \rightarrow T_1$ intersystem crossing (ISC) quantum yields, T_1-state lifetimes that exceed 1 μs, and high oscillator strength $T_1 \rightarrow T_n$ absorptive manifolds that extend over a broad 850–1350 nm spectral window.

2. Experimental Section

Synthesis and Characterization. A full account of the synthesis and characterization of all new compounds, complete with detailed reaction schemes, is provided in the Supporting Information.

Instrumentation. Electronic spectra were recorded on a Shimadzu UV-1700 spectrophotometer. Emission spectra were recorded on a SPEX Fluorolog luminescence spectrometer that utilized a T-channel configuration and R2658 PMT (200–900 nm)/Electro-Optical Systems, Inc. and DSS-16AO20L InGaAs

---

CHART 1: Structures of Bis- and Tris(porphinato)metal(II) Arrays PZn$_n$, PPd$_n$, and PPt$_n$ (n = 2, 3)

M = Zn, R$_x$ = R$_2$ [PZn$_2$]
M = Pd, R$_x$ = R$_1$ [PPd$_2$]
M = Pt, R$_x$ = R$_1$ [PPt$_2$]

M = Zn, R$_x$ = R$_2$, R$_y$ = R$_3$ [PZn$_3$]
M = Pd, R$_x$ = R$_y$ = R$_1$ [PPd$_3$]
M = Pt, R$_x$ = R$_y$ = R$_1$ [PPt$_3$]

R$_1$ =   R$_2$ =   R$_3$ =

(800−1200 nm) detectors; these spectra were corrected using the spectral output of a calibrated light source. Low temperature (77 K) spectra were determined using an optical dewar. NMR spectra were recorded on 250 MHz AMX-250 or 500 MHz AMX-500 Brüker spectrometers. Microwave reactions were performed using a Personal Chemistry Creator (now Biotage) utilizing custom glass reaction vessels.

Transient Absorption Spectroscopy. The femtosecond[54] and nanosecond[55] transient optical systems used for the experiments in this work have been described previously. All samples that were interrogated via transient pump−probe spectroscopic methods were deoxygenated via three successive freeze−pump−thaw cycles prior to measurement.

X-ray Crystal Structures. Dr. Patrick J. Carroll of the X-ray diffraction facility at the University of Pennsylvania solved the structures for compounds described in this work. **PPd$_2$** and **PPt$_2$** crystals were grown from dichloromethane solution layered with methanol. The two solvents slowly diffused followed by slow evaporation. X-ray quality crystals were grown after 2 weeks. A full description of the details and results of these structure determinations is provided in the Supporting Information.

Electrochemistry. Cyclic and square wave voltammetry were carried out on an EG&G Princeton Applied Research model 273A potentiostat/galvanostat. The electrochemical cell utilized a glassy carbon disk working electrode, a platinum wire counter electrode, and a saturated calomel reference electrode (SCE). The reference electrode was separated from the bulk solution by a junction bridge filled with the corresponding solvent/supporting electrolyte solution. The ferrocene/ferrocenium redox couple was utilized as an internal potentiometric standard.

3. Results and Discussion

The highly conjugated palladium(II)- (**PPd$_n$**) and platinum(II)-containing (**PPt$_n$**) porphyrin arrays described in Chart 1 feature a meso-to-meso ethyne-bridged linkage topology; a large body of experimental data demonstrates that the strong electronic coupling mediated by this multiporphyrin linkage motif creates unusually polarizable and hyperpolarizable structures.[53,54,56−79] The syntheses of **PPd$_2$**, **PPd$_3$**, **PPt$_2$**, and **PPt$_3$** were accomplished through metal-mediated cross-coupling of appropriately brominated and *meso*-ethyne-functionalized (porphinato)zinc(II) precursors.[57,63,80,81] Scheme 1 highlights the synthetic route to the **PPd$_2$** and **PPt$_2$** structures, while the analogous path to the **PPd$_3$** and **PPt$_3$** species is shown in Scheme S1 of the Supporting Information. Following the syntheses of the parent **PZn$_2$** and **PZn$_3$** complexes, these species were demetalated to generate the corresponding free-base complexes (**PFb$_n$**). **PPd$_n$** and **PPt$_n$** complexes were synthesized in high yield from their corre-

sponding **PFb$_n$** precursors via microwave-assisted synthesis (Supporting Information).
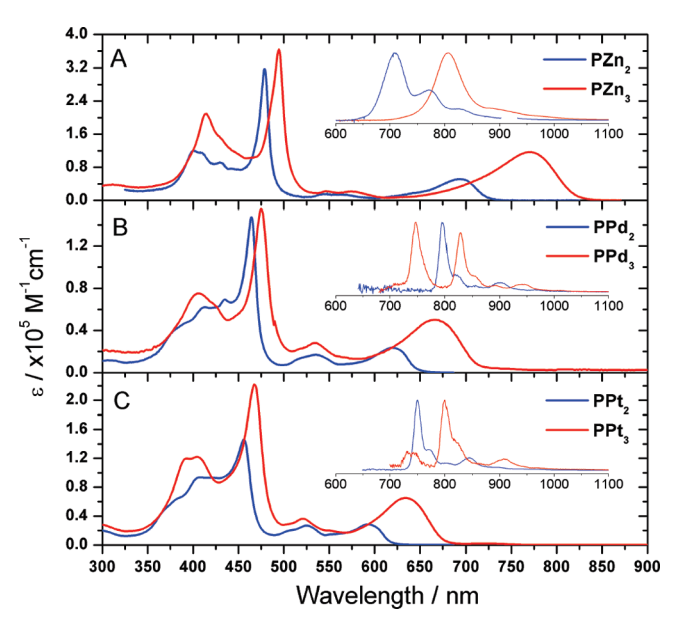
Previous work has demonstrated that **PZn$_n$** conjugated porphyrin arrays manifest low energy Q-state derived $\pi-\pi^*$ excited states that are polarized exclusively along the respective long molecular axes.[53,54,56,57,59,63,66,69,72,75] The lowest energy optical transitions of these species gain in intensity and shift progressively to the red with increasing numbers of conjugated porphyrin units. The electronic absorption spectral data acquired for **PPd$_2$**, **PPd$_3$**, **PPt$_2$**, and **PPt$_3$** (Figure 1, Table 1) manifest the general spectroscopic characteristics delineated previously for the corresponding **PZn$_2$** and **PZn$_3$** benchmarks. Note that all of the **PPd$_n$** and **PPt$_n$** species display high oscillator strength Q-state derived low energy $\pi-\pi^*$ absorption bands, with a molar extinction coefficient exceeding 65 000 M^{-1} cm^{-1} for **PPt$_3$**. The spectra in Figure 1 demonstrate that compared to the analogous **PZn$_n$** spectroscopic benchmarks, the Q-state derived electronic absorption bands for the palladium and platinum derivatives are blue-shifted; this phenomenon is common to *hypso*porphyrin species and has been attributed to efficient mixing of the porphyrin π^* and metal nd_π orbitals.[82−84] Furthermore, X-ray crystallographic data (Supporting Information) show that **PPd$_2$** and **PPt$_2$** access not only conformations in which the adjacent porphyrin least-squares planes do not share a common plane but also those where the $C_{meso}-C_{\alpha\text{-ethyne}}-C_{\beta\text{-ethyne}}$ angle deviates significantly from 180° (**PPd$_2$** = 173.8°; **PPt$_2$** = 172.0°); it is well established within this class of chromophores[54,59,66] that such structural conformers augment the magnitude of Q$_x$-state absorption oscillator strength that is blue-shifted with respect to that which corresponds to the maximally conjugated conformer.

Emission spectra recorded at 77 K in glassy 2-methyltetrahydrofuran (MTHF) solvent for **PPd$_n$** and **PPt$_n$**, as well as for the **PZn$_n$** benchmarks, are depicted in the Figure 1 insets. The palladium and platinum species manifest well-resolved phosphorescence (T$_1$ → S$_0$) transitions at 77 K, approximately 3000 cm^{-1} red-shifted from their respective lowest-energy ground-state singlet absorption band maxima; note that these chromophores contrast their respective zinc analogues, which exhibit no observable phosphorescence, even at 77 K.[54,58] The observed phosphorescence in the palladium and platinum compounds derives in part from the efficient S$_1$ → T$_1$ intersystem crossing (ISC) facilitated by the large spin−orbit coupling constants of these heavy central metal ions.[51,84] It is important to note, however, that even at 77 K, phosphorescence for **PPd$_n$** and **PPt$_n$** is weak (phosphorescence quantum yields, ϕ_p, were estimated by comparison to fluorescent (porphinato)zinc benchmarks to be below 5%). Note also that **PPd$_3$** and **PPt$_3$** also exhibit residual fluorescence (S$_1$ → S$_0$) bands (Table 1); excitation spectra evince that this fluorescence is authentic and does not derive from residual free-base impurities.

Pump−probe femtosecond transient absorption spectroscopy was employed to investigate the absorptive properties and relaxation dynamics of the **PPd$_n$** and **PPt$_n$** excited states. Representative transient absorption spectra recorded at various time delays are shown in Figure 2 (**PPd$_2$**, **PPt$_2$**) and Figure 3 (**PPd$_3$**, **PPt$_3$**), along with the analogous dynamical data obtained for the corresponding **PZn$_n$** benchmarks.[54,66] The early time-delay transient absorption spectra (t_{delay} < 500 fs, Figures 2 and 3, black lines) of each **PZn$_n$**, **PPd$_n$**, and **PPt$_n$** chromophore share several common features: (a) bleaching signatures of the ground-state Q- and B-state derived bands, (b) transient absorption in the spectral region between these two bleaching signatures, and (c) *intense* excited-state absorption manifolds that extend over

SCHEME 1: Synthetic Reaction Scheme for PZn$_2$, PPd$_2$, and PPt$_2$[a]

[a] Detailed synthetic procedures for these species, as well as for the corresponding trimeric **PZn$_3$**, **PPd$_3$**, and **PPt$_3$** structures, are provided in the Supporting Information.

Figure 1. Electronic absorption spectra recorded for (A) **PZn$_n$**,[63] (B) **PPd$_n$**, and (C) **PPt$_n$** in THF solvent at ambient temperature [$n = 2$ (blue); $n = 3$ (red)]. Insets: normalized emission spectra, recorded in deoxygenated glassy MTHF at 77 K. Excitation wavelengths: (A) 460 nm (**PZn$_n$**), (B) 630 nm (**PPd$_2$**), 650 nm (**PPd$_3$**), and (C) 600 nm (**PPt$_2$**), 640 nm (**PPt$_3$**).

a broad NIR energy regime. At early time delays, the NIR transient absorption signatures (Figure 2) observed for **PZn$_2$**, **PPd$_2$**, and **PPt$_2$** are dominated by respective absorption bands centered at 980 nm (full width at half-maximum (fwhm) = 660 cm^{-1}), 888 nm (fwhm = 930 cm^{-1}), and 848 nm (fwhm = 1580 cm^{-1}). The early time-delay transient spectrum of **PZn$_3$** (Figure 3A) exhibits a NIR absorption band ($\lambda_{max}(S_1 \rightarrow S_n)$) centered at 1120 nm; note that this transition is considerably broader (fwhm = 750 cm^{-1}) than that observed for the analogous early time **PZn$_2$** NIR transient (fwhm = 670 cm^{-1}), and that the **PZn$_3$** $S_1 \rightarrow S_n$ spectra also feature a higher energy NIR absorption centered manifold at ~980 nm. In contrast, for **PPd$_3$** and **PPt$_3$**

the low energy transient absorption manifolds observed at t_{delay} < 350 fs are significantly broader than that evinced for **PZn$_3$**. In this regard, note that **PPd$_3$** and **PPt$_3$** feature prominent transient absorption maxima evident at 984 and ~940 nm[85] (Figure 3B,C), respectively; while these highest extinction $S_1 \rightarrow S_n$ absorption manifolds are considerably blue-shifted relative to that of the **PZn$_3$** benchmark, note that both **PPd$_3$** and **PPt$_3$** also display absorption manifolds that extend beyond 1100 nm. Factors that contribute to the more complex nature of the early t_{delay} **PPd$_3$** and **PPt$_3$** transient absorption spectra likely include the augmented degree of conformational inhomogeneity of these species relative to that demonstrated previously for **PZn$_3$**, and Pd(II) and Pt(II) d-orbital/porphyrin π^*-orbital mixing that enables spectral contributions from transitions between states that involve spin multiplicities higher than singlet.

Figures 2A and 3A show that for electronically excited **PZn$_2$** and **PZn$_3$**, the S_1 state persists for several hundred picoseconds;[86] after this time, ground-state bleaching and $S_1 \rightarrow S_n$ excited-state absorption manifold intensities greatly diminish, and weak absorption bands evolve at significantly lower energies (**PZn$_2$**, 1017 nm; **PZn$_3$**, 1196 nm) than those of the $S_1 \rightarrow S_n$ peak maxima. The formation of these new NIR absorptive features is accompanied by the disappearance of the stimulated emission contributions to the respective bleaching signals for these **PZn$_n$** species, which contribute significantly to the observed bleach intensity at early time delays. As a result of these considerations, the long-wavelength **PZn$_n$** transient absorption bands observed at t_{delay} > ~100 ps are assigned to transitions between excited triplet states; however, the weak intensity of these $T_1 \rightarrow T_n$ transitions, coupled with the near-total loss of the ground-state bleaching signatures at delay times where the $T_1 \rightarrow T_n$ transitions are manifested, indicate that population of the triplet surface is a minor deactivation pathway for ^{1}**PZn$_n$*** species. This conclusion is congruent with related dynamical data that demonstrate that the primary deactivation modes for these ^{1}**PZn$_n$*** chromophores are $S_1 \rightarrow S_0$ internal conversion and fluorescence, and steady-state experiments that show that these NIR fluorophores manifest unusually high fluorescence quantum yields.[54]

TABLE 1: Steady-State Spectroscopic Data of Zinc, Palladium, and Platinum Oligomeric Porphyrin Arrays

	λ_{max} $S_0 \rightarrow S_1$ [nm][a,b] (fwhm, cm^{-1})	ε_g @ $S_0 \rightarrow S_1$ [M^{-1} cm^{-1}][a]	λ_{max} $S_0 \rightarrow S_1$ [nm][c,d] (Stokes shift, cm^{-1})	λ_{max} $T_1 \rightarrow S_0$ [nm][c,e] ($S_0 \rightarrow S_1 - T_1 \rightarrow S_0$, cm^{-1})
PZn₂[f]	695 ($\Delta\nu = 1090$)	51400	711 ($\Delta\nu_{Stokes} = 320$)	g
PPd₂	620 ($\Delta\nu = 1330$)	23540	h	796 ($\Delta\nu = 3570$)
PPt₂	592 ($\Delta\nu = \sim 1030$)	28510	h	750 ($\Delta\nu = 3600$)
PZn₃[f]	770 ($\Delta\nu = 1380$)	116000	806 ($\Delta\nu_{Stokes} = 580$)	g
PPd₃	666 ($\Delta\nu = 2170$)	50100	747 ($\Delta\nu_{Stokes} = 1790$)	828 ($\Delta\nu = 3120$)
PPt₃	634 ($\Delta\nu = 1700$)	65050	~ 740 ($\Delta\nu_{Stokes} = 2220$)	800 ($\Delta\nu = 3260$)

[a] Electronic absorption data were recorded in THF at room temperature. [b] The parenthetical value is the transition manifold spectral breadth (fwhm) in cm^{-1}. [c] Emission data were recorded in glassy MTHF at 77 K. [d] The parenthetical value corresponds to the magnitude of the fluorescence Stokes shift. [e] The parenthetical values correspond to the energy gap between the $S_0 \rightarrow S_1$ absorption and phosphorescence band maxima, in cm^{-1}. [f] Spectroscopic data for **PZn₂** and **PZn₃** were taken from cited references.[54,63,66] [g] No phosphorescence was observed. [h] No fluorescence was observed.
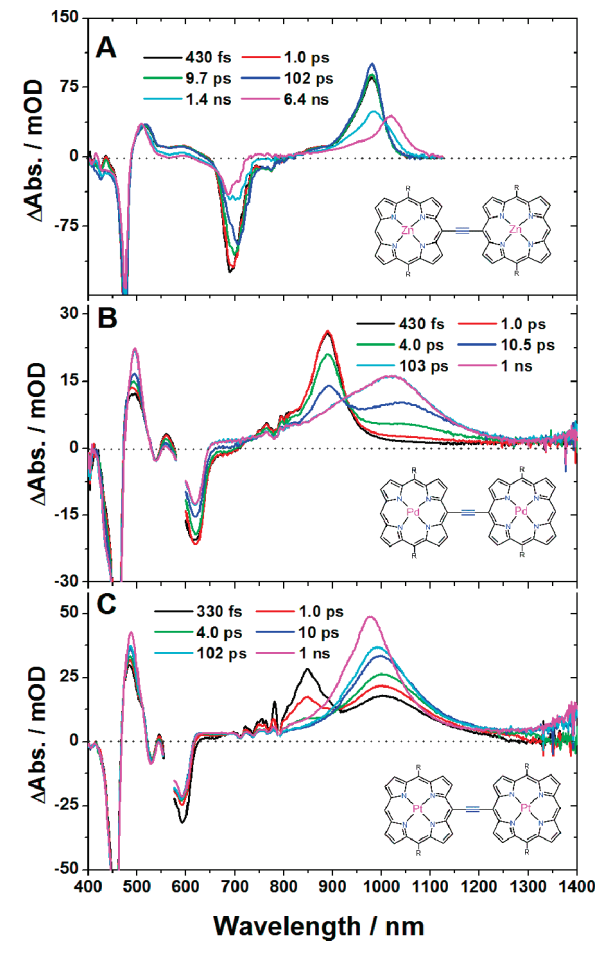

Figure 2. Magic angle transient absorption spectra recorded at selected delay times for (A) **PZn₂**, (B) **PPd₂**, and (C) **PPt₂**. Experimental conditions: solvent = THF, ambient temperature, λ_{exc} = (A) 684 nm, (B) 590 nm, and (C) 560 nm.
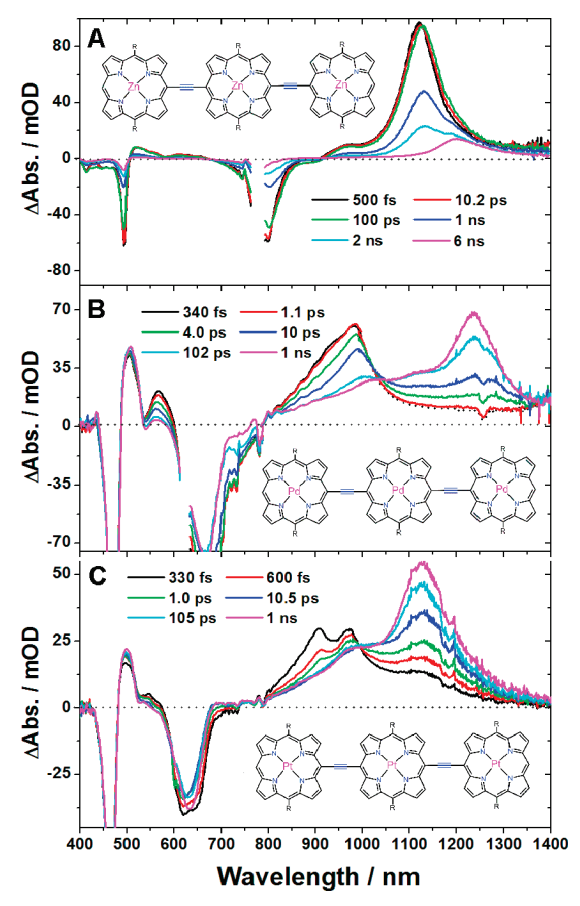

Figure 3. Magic angle transient absorption spectra recorded at selected delay times for (A) **PZn₃**, (B) **PPd₃**, and (C) **PPt₃**. Experimental conditions: solvent = THF, ambient temperature, λ_{exc} = (A) 775 nm, (B) 620 nm, and (C) 600 nm.

Transient spectra of **PPd**_n_ and **PPt**_n_ observed at later time delays ($t_{delay} > 4$ ps, Figures 2B,C and 3B,C) differ markedly from those of the **PZn**_n_ benchmarks. As observed in the **PZn**_n_ transient absorption data, the excited-state spectra of **PPd**_n_ and **PPt**_n_ also evolve at long time-delays to give rise to new transient absorption features that lie 150−200 nm to the red of the $S_1 \rightarrow S_n$ excited-state absorptions. These transient absorption manifolds that persist through the microsecond time domain are likewise assigned to transitions between states of high spin multiplicity ($T_1 \rightarrow T_n$). Unlike the $T_1 \rightarrow T_n$ transition manifold observed for **³PZn**_n_*, the $T_1 \rightarrow T_n$ absorption features for both **PPd**_n_ and **PPt**_n_ are intense and span a broad spectral domain: for example, **³PPd₃*** displays a $T_1 \rightarrow T_n$ absorption manifold

centered at 1235 nm having a fwhm of ~2400 cm^{-1} (Figures 2 and 3; Table 2). It is also noteworthy that the **PPd**_n_ and **PPt**_n_ transient spectra evince ground-state bleaching signatures that remain intense at all delay times (Figures 2−3), even after formation of the excited triplet state is complete ($t_{delay} \sim 6$ ns); these data contrast the analogous pump−probe spectroscopic results obtained for **PZn**_n_ species, and show that T_1-state formation occurs at near-unit quantum yield.

By monitoring the intensification of the **PPd**_n_ and **PPt**_n_ ($T_1 \rightarrow T_n$) transient absorption bands as a function of time delay, the ISC time scales are easily determined; the corresponding exponential time constants (τ_{ISC}) are compiled in Table 2. ISC rates scale inversely with the nuclear charge (Z) of the central metal, with τ_{ISC} (Zn) > τ_{ISC} (Pd) > τ_{ISC} (Pt), consistent with the relative magnitudes of the respective spin−orbit coupling

TABLE 2: Excited-State Spectroscopic Data of Zinc, Palladium, and Platinum Oligomeric Porphyrin Arrays in THF Solvent at Room Temperature

	λ_{max} $S_1 \rightarrow S_n$ [nm][a] (fwhm, cm^{-1})	λ_{max} $T_1 \rightarrow T_n$ [nm][a] (fwhm, cm^{-1})	ε_e @ $T_1 \rightarrow T_n$ [M^{-1} cm^{-1}][b]	τ_{isc} [ps]	τ_T [μs]
PZn$_2$[c]	980 (670)	1017 (630)	n/a	~7500	n/a
PPd$_2$	888 (930)	1023 (2400)	~31000	8.6	49.4
PPt$_2$	848 (1580)	976 (1280)	~71000	~0.3	8.4
PZn$_3$[c]	1120 (750)	1196 (820)	n/a	>2000[d]	n/a
PPd$_3$	984 (>5000[e])	1235 (1180)	~45000	52.0	33.3
PPt$_3$	906, 972 (>5000[e])	1124 (1230)	~95000	~0.6	5.2

[a] The parenthetical value is the spectral breadth (fwhm) in cm^{-1}. [b] Excited triplet-state extinction coefficients were determined from the ultrafast transient absorption data at $t_{delay} = 1$ ns by a method discussed elsewhere;[52] values for **PZn$_2$** and **PZn$_3$** were not calculated due to the facts that the $T_1 \rightarrow T_n$ transition intensity is weak, and the stimulated emission signal contaminates the Q-band bleaching signal even at a 1 ns time delay. [c] Spectroscopic data for **PZn$_2$** and **PZn$_3$** were taken from the cited references.[58,66,72] [d] There is large uncertainty for τ_{isc} for **PZn$_3$** due to overlap of the excited-state singlet and triplet absorption features and a low ISC quantum yield;[54] thus a lower limit for this value is reported. [e] The $S_1 \rightarrow S_n$ transition manifolds of PPd$_3$ and PPt$_3$ encompass multiple distinct peak maxima extending over a large portion of the measured NIR spectral window.

constants of these metal ions. ISC rates for **PPd$_3$** and **PPt$_3$** are slower than those for the corresponding **PPd$_2$** and **PPt$_2$** species, indicating that S_1-to-T_1 conversion rate constants may continue to diminish with increasing conjugation length. This effect has been verified in benchmark **PZn$_n$** compounds as a function of conjugation length; for example, the measured ISC rate for **PZn$_5$** is so small relative to the corresponding radiative and internal conversion rate constants that its excited triplet state remains virtually unpopulated following $S_0 \rightarrow S_1$ excitation.[54] Because the heavy-atom-derived ISC rates in **PPd$_n$** and **PPt$_n$** species are much faster than the intrinsic[59,66,87,88] porphyrin nonradiative decay processes, ISC quantum yields approach unity, even for the **PPd$_3$** and **PPt$_3$** derivatives; $T_1 \rightarrow T_n$ excited-state absorptions are intense in comparison to those of their **PZn$_n$** analogs at 500 ps < t_{delay} < 50 μs. As a result, the molar absorptivities of the **PPd$_n$** and **PPt$_n$** excited triplet states are universally large, as indicated by the $T_1 \rightarrow T_n$ molar extinction coefficients compiled in Table 1. The value of $\varepsilon_e(\lambda = 1124$ nm) ~ 95 000 M^{-1} cm^{-1} at $t_{delay} = 1$ ns for **PPt$_3$** (Figure 3C) indicates that this compound is one of the most intensely absorbing excited triplet states reported to date in the NIR energy regime.

Anaerobic transient absorption experiments carried out over a nanosecond−microsecond time scale were utilized to determine the lifetimes of the **PPd$_n$** and **PPt$_n$** excited triplet states (τ_T) described above (Table 1; spectral data are displayed in the Supporting Information, Figures S1−S4). While the triplet lifetimes of these compounds all exceed 5 μs, the data show that τ_T (**PPd$_n$**) is generally longer than the analogous τ_T (**PPt$_n$**) value, reflecting the trend in the τ_{ISC} values noted above. While the lifetimes of the **PPd$_3$** and **PPt$_3$** are shorter than their **PPd$_2$** and **PPt$_2$** counterparts in agreement with the energy gap law,[49,89] it is important to underscore that the extent to which τ_T diminishes with increasing conjugation length is modest for a given metal ion: it is anticipated that **PPd$_n$** and **PPt$_n$** species having longer conjugation lengths will afford further modulation of the OPL window while maintaining T_1 states having microsecond lifetimes.

Carrying out similar pump−probe experiments under aerobic conditions results in efficient excited-state quenching (complete ground-state recovery within 1 μs), as expected for states with high spin multiplicity.[51] It is noteworthy that these **PPd$_n$** and **PPt$_n$** T_1 lifetimes are comparable to or exceed the triplet-state lifetimes of a variety of metal(II) naphthalocyanines that are currently being utilized for OPL applications in the visible regime.[7]

4. Conclusion

In conclusion, we have demonstrated that coupled oscillator photophysics can be exploited to fabricate supermolecular chromophores that possess intense excited-state absorption bands over broad spectral regions of the NIR. In these systems, the large spin−orbit coupling has been utilized to drive near-quantitative yield of the electronically excited triplet states of **PPd$_n$** and **PPt$_n$** species, which possess spectacular, intense, broad absorptivity over technologically important spectral domains of the NIR. While intense NIR excited-state absorption features in heavy-metal containing multimeric porphyrin complexes have been reported before,[47,52,53] it is clear that **PPd$_n$** and **PPt$_n$** structures offer unique flexibility with respect to tuning the position of maximum excited-state absorptivity while assuring microsecond T_1-state lifetimes. For sequential one-photon absorptive processes, **PPd$_2$**, **PPt$_2$**, **PPd$_3$**, and **PPt$_3$** chromophores evince enormous excited-state absorptive extinction coefficients (30 000−100 000 M^{-1} cm^{-1}) at λ_{max} values that range from 970 to 1235 nm. Given that the lifetimes of these species range from 5 to 50 μs, coupled with the fact the full widths at half-maximum of their $T_1 \rightarrow T_n$ absorptive manifolds span 1200−2400 cm^{-1}, **PPd$_n$** and **PPt$_n$** structures define a new precedent for conjugated materials that feature low-lying electronically excited states that are purely $\pi - \pi^*$ in nature for NIR optical limiting and related long-wavelength NLO applications.

Supporting Information Available: Synthetic and characterization details; X-ray crystallographic data for **PPd$_2$** and **PPt$_2$**; microsecond time domain transient absorption data. This material is available free of charge via the Internet at http://pubs.acs.org.

References and Notes

(1) Tutt, L. W.; Boggess, T. F. *Prog. Quant. Electron.* **1993**, *17*, 299–338.

(2) Wang, J.; Blau, W. J. *J. Opt. A. Pure Appl. Opt.* **2009**, *11*, 024001/1−024001/16.

(3) Shirk, J. S.; Pong, R. G. S.; Bartoli, F. J.; Snow, A. W. *Appl. Phys. Lett.* **1993**, *63*, 1880−1882.

(4) Perry, J. W.; Mansour, K.; Lee, I.-Y. S.; Wu, X.-L.; Bedworth, P. V.; Chen, C.-T.; Ng, D.; Marder, S. R.; Miles, P.; Wada, T.; Tian, M.; Sasabe, H. *Science* **1996**, *273*, 1533−1536.

(5) de la Torre, G.; Vázquez, P.; Agulló-López, F.; Torres, T. *Chem. Rev.* **2004**, *104*, 3723−3750.

(6) Nitschke, C.; O'Flaherty, S. M.; Kröll, M.; Blau, W. J. *J. Phys. Chem. B* **2004**, *108*, 1287−1295.

(7) Chen, Y.; Hanack, M.; Araki, Y.; Ito, O. *Chem. Soc. Rev.* **2005**, *34*, 517−529.

(8) Dini, D.; Calvete, M. J. F.; Hanack, M.; Meneghetti, M. *J. Phys. Chem. A* **2008**, *112*, 8515−8522.

(9) Zhang, L.; Wang, L. *J. Mater. Sci.* **2008**, *43*, 5692−5701.

(10) Chen, Y.; Gao, L.; Feng, M.; Gu, L.; He, N.; Wang, J.; Araki, Y.; Blau, W. J.; Ito, O. *Mini-Rev. Org. Chem.* **2009**, *6*, 55−65.

(11) Manaa, H.; Al Mulla, A.; Makhseed, S.; Al-sawah, M.; Samuel, J. *Opt. Mater.* **2009**, *32*, 108−114.

(12) Chen, P.; Tomov, I. V.; Dvornikov, A. S.; Nakashima, M.; Roach, J. F.; Alabran, D. M.; Rentzepis, P. M. *J. Phys. Chem.* **1996**, *100*, 17507−17512.

(13) Su, W.; Cooper, T. M.; Brant, M. C. *Chem. Mater.* **1998**, *10*, 1212−1213.

(14) Pandey, R. K.; Sandeep, C. S. S.; Philip, R.; Lakshminarayanan, V. *J. Phys. Chem. C* **2009**, *113*, 8630−8634.

(15) Tutt, L. W.; Kost, A. *Nature* **1992**, *356*, 225−226.

(16) Brusatin, G.; Signorini, R. *J. Mater. Chem.* **2002**, *12*, 1964−1977.

(17) Goh, H.-W.; Goh, S. H.; Xu, G. Q.; Lee, K. Y.; Yang, G. Y.; Lee, Y. W.; Zhang, W.-D. *J. Phys. Chem. B* **2003**, *107*, 6056−6062.

(18) Iliopoulos, K.; Couris, S.; Hartnagel, U.; Hirsch, A. *Chem. Phys. Lett.* **2007**, *448*, 243−247.

(19) Mountrichas, G.; Pispas, S.; Xenogiannopoulou, E.; Aloukos, P.; Couris, S. *J. Phys. Chem. B* **2007**, *111*, 4315−4319.

(20) Ouyang, X.; Zeng, H.; Ji, W. *J. Phys. Chem. B* **2009**, *113*, 14565−14573.

(21) Chin, K. C.; Gohel, A.; Chen, W. Z.; Elim, H. I.; Ji, W.; Chong, G. L.; Sow, C. H.; Wee, A. T. S. *Chem. Phys. Lett.* **2005**, *409*, 85−88.

(22) Chen, Y.; Lin, Y.; Liu, Y.; Doyle, J.; He, N.; Zhuang, X.; Bai, J.; Blau, W. J. *J. Nanosci. Nanotechnol.* **2007**, *7*, 1268−1283.

(23) Chen, Y.; Muthukumar, V. S.; Wang, Y.; Li, C.; Krishnan, S. S.; Sai, S. S. S.; Venkataramaniah, K.; Mitra, S. *J. Mater. Chem.* **2009**, *19*, 6568−6572.

(24) Wang, J.; Chen, Y.; Blau, W. J. *J. Mater. Chem.* **2009**, *19*, 7425−7443.

(25) Zhang, L.; Allen, S. D.; Woelfle, C.; Zhang, F. J. *J. Phys. Chem. C* **2009**, *113*, 13979−13984.

(26) Wang, G.; Sun, W. *J. Phys. Chem. B* **2006**, *110*, 20901−20905.

(27) Venkatram, N.; Kumar, R. S. S.; Rao, D. N. *J. Appl. Phys.* **2006**, *100*, 074309/1−8.

(28) Martin, R. B.; Meziani, M. J.; Pathak, P.; Riggs, J. E.; Cook, D. E.; Perera, S.; Sun, Y.-P. *Opt. Mater.* **2007**, *29*, 788−793.

(29) Yu, X.-L.; Cao, C.-B.; Zhu, H.-S.; Li, Q.-S.; Liu, C.-L.; Gong, Q.-H. *Adv. Funct. Mater.* **2007**, *17*, 1397−1401.

(30) Zhu, J. *Appl. Opt.* **2008**, *47*, 5848−5852.

(31) Li, Q.; Liu, C.; Zang, L.; Gong, Q.; Yu, X.; Cao, C. *J. Opt. Soc. Am. B-Opt. Phys.* **2008**, *25*, 1978−1983.

(32) Singh, C. P.; Bindra, K. S.; Bhalerao, G. M.; Oak, S. M. *Opt. Exp.* **2008**, *16*, 8440−8450.

(33) Patra, A.; Venkatram, N.; Rao, D. N.; Radhakrishnan, T. P. *J. Phys. Chem. C* **2008**, *112*, 16269−16274.

(34) Polavarapu, L.; Venkatram, N.; Ji, W.; Xu, Q.-H. *ACS Appl. Mater. Int.* **2009**, *1*, 2298−2303.

(35) Pan, H.; Chen, W.; Feng, Y. P.; Ji, W.; Lin, J. *Appl. Phys. Lett.* **2006**, *88*, 223106/1−3.

(36) Zhou, G.-J.; Wong, W.-Y.; Lin, Z.; Ye, C. *Angew. Chem., Int. Ed.* **2006**, *45*, 6189−6193.

(37) Zhou, G.-J.; Wong, W.-Y.; Ye, C.; Lin, Z. *Adv. Funct. Mater.* **2007**, *17*, 963−975.

(38) Zheng, Q.; Gupta, S. K.; He, G. S.; Tan, L.-S.; Prasad, P. N. *Adv. Funct. Mater.* **2008**, *18*, 2770−2779.

(39) Girardot, C.; Cao, B.; Mulatier, J.-C.; Baldeck, P. L.; Chauvin, J.; Riehl, D.; Delaire, J. A.; Andraud, C.; Lemercier, G. *Chem. Phys. Chem.* **2008**, *9*, 1531−1535.

(40) Manjunatha, M. G.; Adhikari, A. V.; Hegde, P. K.; Sandeep, C. S. S.; Philip, R. *J. Mater. Sci.* **2009**, *44*, 6069−6077.

(41) Kamanina, N. V.; Voronin, Y. M.; Varnaev, A. V.; Bagrov, I. V.; Zhevlakov, A. P. *Synth. Met.* **2003**, *138*, 317−322.

(42) Lin, T.-C.; He, G. S.; Zheng, Q.; Prasad, P. N. *J. Mater. Chem.* **2006**, *16*, 2490−2498.

(43) Bouit, P.-A.; Wetzel, G.; Berginc, G.; Loiseaux, B.; Toupet, L.; Feneyrou, P.; Bretonnière, Y.; Kamada, K.; Maury, O.; Andraud, C. *Chem. Mater.* **2007**, *19*, 5325−5335.

(44) Li, F.; Zheng, Q.; Yang, G.; Dai, N.; Lu, P. *Mater. Lett.* **2008**, *62*, 3059−3062.

(45) Lin, T.-C.; Chen, Y.-F.; Hu, C.-L.; Hsu, C.-S. *J. Mater. Chem.* **2009**, *19*, 7075−7080.

(46) Zheng, Q.; He, G. S.; Prasad, P. N. *Chem. Phys. Lett.* **2009**, *475*, 250−255.

(47) Hales, J. M.; Cozzuol, M.; Screen, T. E. O.; Anderson, H. L.; Perry, J. W. *Opt. Exp.* **2009**, *17*, 18478−18488.

(48) Bouit, P.-A.; Westlund, R.; Feneyrou, P.; Maury, O.; Malkoch, M.; Malmström, E.; Andraud, C. *New J. Chem.* **2009**, *33*, 964−968.

(49) Englman, R.; Jortner, J. *Mol. Phys.* **1970**, *18*, 145.

(50) Caspar, J. V.; Meyer, T. J. *J. Phys. Chem.* **1983**, *87*, 952−957.

(51) Turro, N. J. *Modern Molecular Photochemistry*; University Science Books: Sausolito, CA, 1991.

(52) Duncan, T. V.; Rubtsov, I. V.; Uyeda, H. T.; Therien, M. J. *J. Am. Chem. Soc.* **2004**, *126*, 9474−9475.

(53) Duncan, T. V.; Ishizuka, T.; Therien, M. J. *J. Am. Chem. Soc.* **2007**, *129*, 9691−9703.

(54) Duncan, T. V.; Susumu, K.; Sinks, L. E.; Therien, M. J. *J. Am. Chem. Soc.* **2006**, *128*, 9000−9001.

(55) Papp, S.; Vanderkooi, J. M.; Owen, C. S.; Holtom, G. R.; Phillips, C. M. *Biophys. J.* **1990**, *58*, 177−186.

(56) Lin, V. S.-Y.; DiMagno, S. G.; Therien, M. J. *Science* **1994**, *264*, 1105−1111.

(57) Lin, V. S.-Y.; Therien, M. J. *Chem.−Eur. J.* **1995**, *1*, 645−651.

(58) Angiolillo, P. J.; Lin, V. S.-Y.; Vanderkooi, J. M.; Therien, M. J. *J. Am. Chem. Soc.* **1995**, *117*, 12514−12527.

(59) Kumble, R.; Palese, S.; Lin, V. S.-Y.; Therien, M. J.; Hochstrasser, R. M. *J. Am. Chem. Soc.* **1998**, *120*, 11489−11498.

(60) Fletcher, J. T.; Therien, M. J. *J. Am. Chem. Soc.* **2000**, *122*, 12393−12394.

(61) Shediac, R.; Gray, M. H. B.; Uyeda, H. T.; Johnson, R. C.; Hupp, J. T.; Angiolillo, P. J.; Therien, M. J. *J. Am. Chem. Soc.* **2000**, *122*, 7017−7033.

(62) Angiolillo, P. J.; Susumu, K.; Uyeda, H. T.; Lin, V. S.-Y.; Shediac, R.; Therien, M. J. *Synth. Met.* **2001**, *116*, 247−253.

(63) Susumu, K.; Therien, M. J. *J. Am. Chem. Soc.* **2002**, *124*, 8550−8552.

(64) Fletcher, J. T.; Therien, M. J. *J. Am. Chem. Soc.* **2002**, *124*, 4298−4311.

(65) Fletcher, J. T.; Therien, M. J. *Inorg. Chem.* **2002**, *41*, 331−341.

(66) Rubtsov, I. V.; Susumu, K.; Rubtsov, G. I.; Therien, M. J. *J. Am. Chem. Soc.* **2003**, *125*, 2687−2696.

(67) Ostrowski, J. C.; Susumu, K.; Robinson, M. R.; Therien, M. J.; Bazan, G. C. *Adv. Mater.* **2003**, *15*, 1296−1300.

(68) Angiolillo, P. J.; Uyeda, H. T.; Duncan, T. V.; Therien, M. J. *J. Phys. Chem. B* **2004**, *108*, 11893−11903.

(69) Susumu, K.; Duncan, T. V.; Therien, M. J. *J. Am. Chem. Soc.* **2005**, *127*, 5186−5195.

(70) Ghoroghchian, P. P.; Frail, P. R.; Susumu, K.; Blessington, D.; Brannan, A. K.; Bates, F. S.; Chance, B.; Hammer, D. A.; Therien, M. J. *Proc. Natl. Acad. Sci. U.S.A.* **2005**, *102*, 2922−2927.

(71) Ghoroghchian, P. P.; Frail, P. R.; Susumu, K.; Park, T.-H.; Wu, S. P.; Uyeda, H. T.; Hammer, D. A.; Therien, M. J. *J. Am. Chem. Soc.* **2005**, *127*, 15388−15390.

(72) Duncan, T. V.; Wu, S. P.; Therien, M. J. *J. Am. Chem. Soc.* **2006**, *128*, 10423−10435.

(73) Susumu, K.; Frail, P. R.; Angiolillo, P. J.; Therien, M. J. *J. Am. Chem. Soc.* **2006**, *128*, 8380−8381.

(74) Frail, P. R.; Susumu, K.; Huynh, M.; Fong, J.; Kikkawa, J. M.; Therien, M. J. *Chem. Mater.* **2007**, *19*, 6062−6064.

(75) Keinan, S.; Therien, M. J.; Beratan, D. N.; Yang, W. T. *J. Phys. Chem. A* **2008**, *112*, 12203−12207.

(76) Duncan, T. V.; Ghoroghchian, P. P.; Rubtsov, I. V.; Hammer, D. A.; Therien, M. J. *J. Am. Chem. Soc.* **2008**, *130*, 9773−9784.

(77) Duncan, T. V.; Song, K.; Hung, S. T.; Miloradovic, I.; Nayak, A.; Persoons, A.; Verbiest, T.; Therien, M. J.; Clays, K. *Angew. Chem., Int. Ed.* **2008**, *47*, 2978−2981.

(78) Fisher, J. A. N.; Susumu, K.; Therien, M. J.; Yodh, A. G. *J. Chem. Phys.* **2009**, *130*, 134506/1−8.

(79) Banerjee, P.; Conklin, D.; Nanayakkara, S.; Park, T.-H.; Therien, M. J.; Bonnell, D. A. *ACS Nano* **2010**, *4*, 1019−1025.

(80) DiMagno, S. G.; Lin, V. S.-Y.; Therien, M. J. *J. Org. Chem.* **1993**, *58*, 5983−5993.

(81) DiMagno, S. G.; Lin, V. S.-Y.; Therien, M. J. *J. Am. Chem. Soc.* **1993**, *115*, 2513−2515.

(82) Eastwood, D.; Gouterman, M. *J. Mol. Spectrosc.* **1970**, *35*, 359.

(83) *Optical Spectra and Electronic Structure of Porphyrins*; Gouterman, M., Ed.; Academic Press: New York, 1978; Vol. 3.

(84) Harriman, A. *J. Chem. Soc., Faraday Trans. 2* **1981**, *77*, 1281–1291.

(85) The $S_1 \rightarrow S_n$ transition manifold exhibits two well-resolved transitions of nearly equal intensity (Table 2); 940 nm represents an average position.

(86) There are some moderate-scale excitation-wavelength-dependent changes to the spectral features that occur on a 15−30 ps time scale. These changes are generally associated with structural relaxation around the ethyne bridge, with excited electronic-state conformeric populations favoring smaller average macrocycle−macrocycle dihedral angles than those of the ground electronic state.

(87) Baskin, J. S.; Yu, H.-Z.; Zewail, A. H. *J. Phys. Chem. A* **2002**, *106*, 9837–9844.

(88) Wynne, K.; LeCours, S. M.; Galli, C.; Therien, M. J.; Hochstrasser, R. M. *J. Am. Chem. Soc.* **1995**, *117*, 3749–3753.

(89) Caspar, J. V.; Meyer, T. J. *J. Phys. Chem.* **1983**, *87*, 952–957.